A High-Throughput Biophotonics Instrument to Screen for Novel Ocular Photosensitizing Therapeutic Agents

Mark C. Butler,[1] *Patrick N. Itotia,*[1,2] *and Jack M. Sullivan*[1,2,3,4,5,6]

Purpose. High-throughput techniques are needed to identify and optimize novel photodynamic therapy (PDT) agents with greater efficacy and to lower toxicity. Novel agents with the capacity to completely ablate pathologic angiogenesis could be of substantial utility in diseases such as wet age-related macular degeneration (AMD).

Methods. An instrument and approach was developed based on light-emitting diode (LED) technology for high-throughput screening (HTS) of libraries of potential chemical and biological photosensitizing agents. Ninety-six-well LED arrays were generated at multiple wavelengths and under rigorous intensity control. Cell toxicity was measured in 96-well culture arrays with the nuclear dye SYTOX Green (Invitrogen-Molecular Probes, Eugene, OR).

Results. Rapid screening of photoactivatable chemicals or biological molecules has been realized in 96-well arrays of cultured human cells. This instrument can be used to identify new PDT agents that exert cell toxicity on presentation of light of the appropriate energy. The system is further demonstrated through determination of the dose dependence of model compounds having or lacking cellular phototoxicity. Killer Red (KR), a genetically encoded red fluorescent protein expressed from transfected plasmids, is examined as a potential cellular photosensitizing agent and offers unique opportunities as a cell-type–specific phototoxic protein.

Conclusions. This instrument has the capacity to screen large chemical or biological libraries for rapid identification and optimization of potential novel phototoxic lead candidates. KR and its derivatives have unique potential in ocular gene therapy for pathologic angiogenesis or tumors. (*Invest Ophthalmol Vis Sci.* 2010;51:2705–2720) DOI:10.1167/iovs.08-2862

Treatment of retinal and choroidal angiogenesis with light has a history in xenon arc therapy, laser panretinal photocoagulation, and focal extrafoveal macular treatments, and has reached its current state of technological development in photodynamic therapy (PDT). PDT involves the use of a small photosensitizing molecule (generally, <500 Da) with optical activity. Singlet oxygen ($^1O_2$) is generated inside or near cells on absorption of light of a specific energy band that couples into the molecular absorption dipole.[1] Photosensitizing molecules absorb a photon of appropriate energy to form a singlet state that progresses to the triplet state by intersystem transfer. From the triplet state, the molecule reacts with molecular oxygen (O_2) through energy transfer mechanisms to generate $^1O_2$.[2] Singlet oxygen can exert toxicity at several cellular levels. Macromolecules can exhibit such photochemical behavior as well.[3] Within the target cells of PDT—the vascular endothelial cells (VECs) involved in pathologic angiogenesis—reactive oxygen species (ROS) promote membrane damage, mitochondrial toxicity, and cell death. Singlet oxygen generated by light has an extremely short half-life (~20 ns), and its mobility is diffusion-limited, so that the molecular targets of toxicity must reside within very short distances (~20 nm) of the activated photosensitizing agent. One set of PDT agents is made up of optically active compounds called porphyrins.[1] Verteporfin (Visudyne; Novartis, East Hanover, NJ) has been the pinnacle of achievement for clinical PDT technology for application to pathologic angiogenesis in the human eye, such as wet AMD caused by choroidal neovascular (CNV) membranes. Verteporfin has been shown to slow progression of vision loss in patients with predominantly classic CNV.[4–6] It is a liposomal preparation of a benzoporphyrin acid derivative[7] that is injected by an intravenous route and is thought to have a longer sojourn in the vascular networks of pathologic angiogenesis than in normal capillary vasculature. It is a PDT photosensitizer which, like other PDT agents, is known to act inside cells.[1] It exerts phototoxicity at the level of the plasma membrane and mitochondrial membranes on light excitation. On photoactivation with far-red light (692 nm) verteporfin generates $^1O_2$ in the immediate environment of the small, hemelike molecules. Because PDT agents tend to be hydrophobic compounds, they are absorbed into many cells including VECs of the normal vasculature. Clearly one of the major problems with PDT is the lack of specificity. Any cell type that takes up the agent and is exposed to light of the relevant optical bandwidth can sustain toxicity. Verteporfin PDT has demonstrated toxicity on other cell types both within and outside the retina.[8] Patients and their physicians must be concerned about systemic broadband light exposure (e.g., the sun) after retinal PDT for wet AMD, as the potential is high for dermal burns or iatrogenic porphyria. In contrast, the ideal PDT agent is one in which the *only* cell type that is susceptible to phototoxicity is the diseased cell

From the Departments of [1]Ophthalmology, [3]Pharmacology and Toxicology, and [4]Physiology and Biophysics, the [2]Neuroscience Program, and the [5]Ira G. Ross Eye Institute, SUNY University at Buffalo, Buffalo, New York; and the [6]Veterans Administration Western New York Healthcare System, Buffalo, New York.

Supported by a University at Buffalo Interdisciplinary Research Creative Activities Fund (IRCAF) award; National Eye Institute Core Grant R24 EY016662 to the Vision Science group at University at Buffalo (University at Buffalo Vision Infrastructure Center [CORE]), Biophotonics Module 5R24EY016662-039001 (JMS); University at Buffalo Ophthalmology Departmental faculty startup funds (originating from the Oishei Foundation, Buffalo, NY); and challenge and unrestricted grants from Research to Prevent Blindness to the Department of Ophthalmology at the University at Buffalo. The study was conducted in its entirety at the Veterans Administration Western New York Healthcare System.

Submitted for publication September 11, 2008; revised December 15, 2008, and March 6 and May 20, 2009; accepted March 4, 2010.

Disclosure: **M.C. Butler**, None; **P.N. Itotia**, None; **J.M. Sullivan**, None

Corresponding author: Jack M. Sullivan, Associate Professor of Ophthalmology, Pharmacology/Toxicology, and Physiology/Biophysics, University at Buffalo, The Ross Eye Institute, Veterans Administration Western New York Healthcare System, Medical Research, Building 20, Room 245, 3495 Bailey Avenue, Buffalo, NY 14215; jackmsullivanmdphd@yahoo.com.

type that is the target for treatment or elimination (e.g., VECs of pathologic angiogenesis).

Visudyne PDT is substantially less effective in suppressing CNV when compared with recently proven vascular endothelial growth factor (VEGF) inhibitors, such as bevacizumab (Avastin; Genentech, South San Francisco, CA) and ranibizumab (Lucentis; Hoffman-LaRoche, Nutley, NJ).[9–12] Although these agents have shown effectiveness, they require multiple intravitreal injections, and, although they often promote absorption of macular fluid due to CNV, they do not strongly promote involution of the pathologic angiogenesis of the CNV lesion itself, as has also been shown with PDT.[13] There is obvious clinical interest in novel agents for use in CNV and other ocular forms of pathologic angiogenesis that promote definitive ablation of neovascular networks. The ideal photosensitizing agent is one that is highly effective at generating $^1O_2$ at low concentrations and that activates apoptosis or necrosis only in the diseased cells of interest but not surrounding bystander cells and tissues.[8,13–15] No known photosensitizing agent currently satisfies this criterion.[8] Verteporfin is unlikely to be the pinnacle of therapeutic achievement in PDT. New paradigms in treating retinal, choroidal, and ocular angiogenesis with photosensitizing agents and light are needed.

Screening chemical or macromolecular agents for new photosensitizing agents is a lengthy, cumbersome, personnel-intensive, and expensive process. One tool that has appeared for rapid evaluation of new photosensitizing agents for pathologic angiogenesis is the chorioallantoic membrane of the chick egg.[16] This approach hardly offers the capacity for high-throughput screening (HTS) and uses avian and not human tissue. Another tool employs engineered zebrafish that express a red fluorescent protein into the vascular arches of the embryo.[17] The *necessity* of the approach described herein comes from an appreciation of the biocomplexity of novel drug discovery. The number of potential photochemically active compounds (small molecule or macromolecule) is many orders of magnitude larger than the number that can be screened practically by classic approaches (e.g., chick eggs and animal models). In the sunscreen and cosmetics business, HTS based on cultured cells has been used to assess the phototoxicity of a range of chemicals when subjected to high-energy light in the ultraviolet range. A mouse 3T3 cell neutral red uptake assay is used for cytotoxicity assessment after exposure of cells to a sun-lamp–like UV source.[18–20] We sought to improve on this drug discovery process through the development of HTS tools. In this study, we used human embryonic kidney cells (HEK293S) as a convenient resource to test small-molecule model compounds and a macromolecule as photosensitizing agents in a proof-of-principle demonstration of a novel instrument. We capitalized on the diversity of commercially available contemporary LED technology and our experience with optics, photonics, and electronics,[21] to develop an instrument and HTS approach that can be used for discovery of novel photosensitizing agents and optimization of their properties in a range of possible cell types. Demonstrated by proof of principle, the biophotonics instrument described in this study can be further optimized for advanced drug discovery platforms and coupled to robotic platforms for higher sample throughput. It may also be useful in biotechnology applications, to obtain highly selective cell death in culture or in vivo through the use of light.

Photochemical activity is a property of a plethora of chemical and macromolecular classes, but most of these have not been screened to identify new photosensitizing agents. There is incentive for the development of HTS and high content screening (HCS) technologies in novel photosensitizer drug discovery strategies. HTS and HCS have largely replaced classic pharmacology in the identification of lead candidate compounds in drug discovery. In HTS, a large number of compounds must be tested under defined experimental paradigms, which for novel photosensitizing agents means promotion of optical band-limited cytotoxicity. For example, if one chose a particular wavelength range (band of energy) that would be most useful for delivery into the eye (e.g., retina or choroid), then with the instrument described herein, one could set up an HTS of many compounds, to seek agents that promote cytotoxicity on light exposure. In the 96-well LED testing arrays presented in our proof-of-principle instrument model, seeking such agents would constitute an HTS after thousands of compounds had been tested. Our instrument demonstrates the potential for such HTS. With robotic tools, this platform could screen thousands of test compounds per day for light-induced cytotoxicity in diverse optical bandwidths that are limited only by continually emerging LED technology. The same instrument could also be used in HCS of cell arrays, for example, to test lead candidate agents for a combination of output variables (e.g., cytotoxicity, signal pathway activation, and mitochondrial membrane potential) that are relevant to the type of photochemically active agent sought within the optical band of interest. As far as we know, combinatorial HTS and HCS have never been conducted for the identification of novel photosensitizing agents. A preliminary report of these findings has been made (Itotia PN, et al. *IOVS* 2007;48:ARVO E-Abstract 4584).

Materials and Methods

Construction of LED Arrays and a Novel Biophotonics Instrument

An optical LED array was designed and constructed to illuminate cells attached to the substrates of black-walled, 96-well cell culture plates. Ninety-six LED arrays were fashioned from 96-well cell culture plates (353220, Microtest 96-well assay plates; Optilux, black frame, clear bottom, tissue culture–treated, sterile with lid; BD-Falcon, Franklin Lakes, NJ) from which the polystyrene floor was removed, and the wells machined to accommodate 96 LEDs (5 mm diameter) of a given type placed in standard 0.25-in. LED holders that were press fitted into each well. The cell culture array could be placed immediately on top of the LED array; or, an intervening open-well, 96-well plate could be placed between the LED array and the cellular array; or, an intervening array containing optical elements could be placed between the LED array and the cellular array. High-intensity LEDs with distinct spectral emission bands and narrow-output beams (full-width at half maximum [FWHM]: 15–30°) were identified, to construct a set of LED arrays that covered the visible light spectrum, including violet (420–440 nm), blue (470 nm), blue-green (502 nm), green (526–545 nm), yellow (575 nm), amber (592 nm), orange (620 nm), red (625 nm), and white (465/570 nm) as well as a portion of the UV-light spectrum (405 nm). An image of the LED array control platform and a representative LED array (blue, 470 nm), mounted and operational on the top of the instrument are shown (Fig. 1). The properties and manufacturers of the set of LEDs used in the separate color arrays are tabulated (Table 1). We also include examples of other high-intensity, narrow-spatial-band, 5-mm LEDs that could be used in 96-LED arrays, but were not fully tested in this study, or were tested only as discrete elements for output optical wattage.

LEDs were grouped in gangs of either three or four discrete optical elements soldered together in series with single, small (0.125 W) 47-, 68-, or 150-Ω current-limiting metal film resistors, depending on the array design (Fig. 2). The resistors in series on each LED gang provided current limitation at the maximum drive level. The size of the LED series gang (3 or 4 LEDs) was determined by the forward activation voltages (V_f) of the individual LEDs relative to the voltage (12 V) of the DC power supply and the maximum current ratings of the discrete LED elements. LEDs with V_f above 3.0 V were organized into a 32 × 3-LED array structure (total 96), whereas those with V_f less than 3 V were organized into 24 × 4-LED arrays. The LED gangs were wired in parallel for connection to the power supply. A 1000-Ω, 10-turn, linear potentiometer was placed in series with the overall LED parallel array, to provide a larger range of current control and light output. This poten-

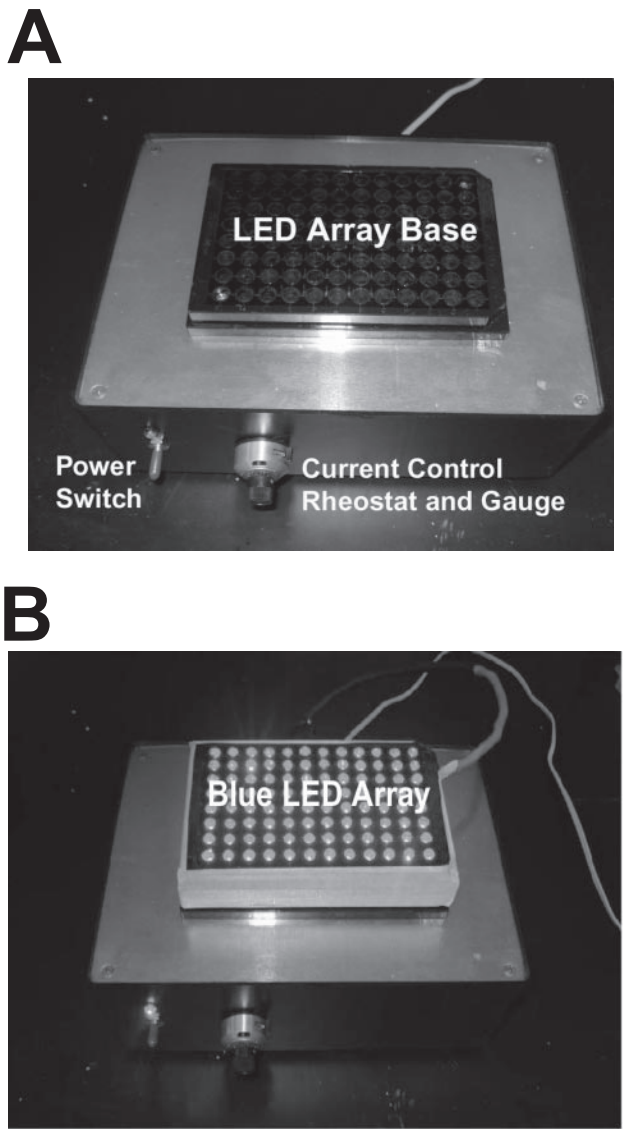

FIGURE 1. (**A**) The LED array driver. The power switch (blue LED indicator) and the current control rheostat and dial gauge monitor are labeled. (**B**) A representative operational blue (470 nm) LED diode array in operation is situated on the control box with optical output near maximum intensity (shown in black and white). A cell culture 96-well array is not present in this image, to allow best visualization of the positioning of the individual LEDs in the array. In most experiments, the cell culture array sat immediately on top of the LED array, whereas in other experiments the energy was concentrated with an intermediate ball lens array that was positioned between the LED array and the cell culture array.

tiometer was panel mounted to provide modulation over the optical output from any attached LED array. A sensitive 10-turn panel dial was attached to the potentiometer to precisely repeat control of LED array current. This HTS 96-LED array device was cooled by forced air flow across the LED array from a DC fan placed in the floor of the device. The device can be used both on the laboratory bench at room temperature and in a cell culture incubator at 37°C. Power to the LED control box came from one of two sources. Initial control came with an inexpensive 12-V DC/1500-mA (18-W) wall adapter (273-1779; Radio Shack, Fort Worth, TX) that was used on the maximum-output setting in all cell phototoxicity experiments reported. However, this power source was not tightly controlled at high current output. We then used a second homemade constant-voltage, constant-current, or constant-wattage DC power supply to drive the LED arrays under rigorous electronic control. This device was built around a commercial 15-V, 13-A linear power supply (model: OLV120-15ELPAC; Power Systems, Irvine, CA) with additional circuitry designed and constructed for power regulation, independent voltage and current control, heat dissipation, and panel display.

The LED power output at the level of the substrate of the cellular array was modulated in one of three independent ways. First, the current through the array was varied through the panel potentiometer. Second, the distance between the LED array and the cellular array could be varied by inserting intervening open-well black culture plates (without a coverslip floor), or by varying the distance between the array and the cell culture surface placed in appropriate register. The radius (r) of the spot of light above the array is governed by the following equation: $\tan \theta = r/d$, where θ is the half-angle of the FWHM spatial band of the LED output, and d is the distance from the surface of the LED array to the cellular array (Fig 3A). The diameter of the spot size was therefore $2r$. The LED chip output was constrained by an intrinsic lens that aided in limiting the divergence of the beam from the chip proper and set up the beam distribution half-angle. Without any intervening apertures or lenses, the intensity of the spot of light varied with the square of distance. The LEDs chosen for the arrays had narrow-beam angles such that the beam would approximately fill a 7-mm diameter tissue culture well (96-well array), when a single, intermediate, open-well tissue culture plate was placed between the LED array and the cell culture plate (Fig. 3B). As the plate was a black-walled cell culture plate, each of the 96 elements served as an optical constraining aperture, thus fixing the size of the spot diameter presented to the cells above at 7 mm, or approximately equal to the diameter of the culture well. Third, a 96-element array of spherical polished acrylic (methyl methacrylate) ball lenses (3.175 mm radius, refractive index = 1.50, sphericity = 0.005 in) (product BL-04; Small Parts Inc., Miramar, FL; Fig. 3B) was generated in a 96-well culture array that was positioned between the LED and cellular arrays, to constrain the divergence of the LED outputs and enhance the optical energy delivery to the cellular surface. The balls were positioned to reside approximately 1 focal length ($F = 3.175$ mm in air) from the cell culture surface, such that they acted to create intense spots of light that underfill the 7-mm well. Spot sizes were in the cellular specimen plane for an open intermediate spacer plate; one filled with ball lenses is shown (Fig. 3C). Intensities delivered to the specimen without and with ball lens were determined (Table 2). The delivery of optical energy to the cellular surface was not attenuated by either standard plastic or glass coverslip culture tray bottoms at all LED wavelengths used in this study (Fig. 3D, Table 1). There was an ~80% transmission of energy by either glass or plastic cell coverslip bottoms at wavelengths above 400 nm (i.e., all arrays in the study).

Light intensity (in milliwatts) of discrete LEDs and the optical output of LED arrays or their output uniformity was measured with a calibrated silicon photodiode (400S) and an optical watt/joule meter (66XLA; 3M Photodyne, Camarillo, CA). The silicon photodiode sensor in the 400S optical head is 7 mm in diameter (model UV-270BQ; EG&G, Inc, Salem, MA) with a circular area of 38.5 mm^2. The diode sensor was placed in a holder mounted directly over the LED to maintain sensor placement at a constant distance from the LED tip, to simulate the distance to the cell culture surface (without intervening spacer or lens arrays). Under these conditions, the maximum LED emission half-angle that would fill the sensor surface is 41.2°, which is greater than the maximum LED half-angle used (30°). As such, the LED output measures (in milliwatts) are reliable without spatial area correction. Each LED output was measured at least three times over the entire range of the DC-based rheostat at every 10th increment.

Cellular Phototoxicity Assay for Small Molecules

To test the ability of LED arrays to identify photosensitizing small molecules capable of cellular toxicity, we chose compounds with known optical properties: tetra-methyl-rhodamine methyl ester per-

TABLE 1. LED Properties

Peak Wave-length (nm)	Color	Manufacturer/Product	Spatial Distribution (FWHM)	Typical Single LED Intensity (mcd)	Measured Single LED Intensity (mW)*
420	Violet	ETG-5AX420-15	15	1,000	2.72 ± 0.09
440	Pink	ETG-5AX440-15	15	1,000	4.20 ± 0.04
470	Blue	Nichia-NSPB510S	30	2,120	4.35 ± 0.01
502	Blue-green	Nichia-NSPE500S	20	9,200	3.07 ± 0.01
525	Green	Nichia-NSPG510S	30	7,200	3.23 ± 0.01
545	Green-yellow	Nichia-NSPG500S	16	16,000	3.56 ± 0.03
575	Yellow	Nichia-NSPY500S	20	6,400	3.97 ± 0.01
592	Amber	Tron-L200CWY6KH-15D	16	6,800	ND
620	Orange	Jameco-333673	12	5,000	1.32 ± 0.01
625	Red	Nichia-NSPR510AS	30	2,800	5.57 ± 0.01
465/570†	White	Nichia-NSPW500CS	16	31,000	9.67 ± 0.02

The peak wavelength of the LED used in the array, the source of the LED, the light distribution view angle (full-width half-maximal), the nominal output (in millicandelas), and the measured mean output (in milliwatts) are shown. Bold items under peak wavelength means that a full 96-array LED was constructed. In other cases, high-intensity LEDs were identified.

* Mean level of LED outputs ± SEM. These values are not corrected for silicon photodiode sensor spectral sensitivity factor. ETG, ETG, Inc. (Los Angeles, CA); Nichia, Nichia Photonics, Inc. (Mountville, PA); Tron, LEDTronic Inc. (Torrance, CA). Jameco, this item originates from Ligitek Corp. (China; Ligitek QW0905-LVX3833D). Discrete LEDs for 420, 440, and 592 nm were tested but not incorporated into LED arrays. The 525- and-545 nm LEDs are both listed by Nichia as green, but the spectral ranks obtained (G for NSPG510S; H for NSPG500S) have chromaticity coordinates that indicate the associated peak wavelengths.

† White emission.

chlorate (TMR), tetra-methyl-rosamine chloride (TMRs), and malachite green carbinol HCl (MG) (T5428-25 mg, T-1823, and Aldrich 213020-25G, respectively; all from Sigma-Aldrich, St. Louis, MO). TMR accumulates in mitochondria and, on photoactivation, induces ROS formation that causes loss of mitochondrial membrane potential and eventual phototoxic apoptosis.[22] TMRs is a triphenylmethane dye structurally similar to TMR and exerts cellular phototoxicity by the same mechanism.[2,23] MG is not toxic to cells at a light dose of 40 J/cm^2 making it a good negative control.[24] All compounds were dissolved in DMSO and stored at −20°C, protected from light. Spectral data on these compounds were obtained from Invitrogen-Molecular Probes (Carlsbad, CA), Web site (http://www.invitrogen.com/site/us/en/home/support/research-tools/fluorescence-spectraviewer.reg.us.html). Chemical structures were drawn in computer software (MDL ISIS/Draw, ver. 2.5; Symyx Corp., Sunnyvale, CA). TMR and TMRs, which are activated efficiently by green light at 526 nm, were compared to MG, which absorbs in the red but not significantly in the green portion of the visible spectrum. HEK293S cells[25] (~50,000 cells/well) were plated onto 96-well, black-walled, cell culture–treated plates (Optilux; BD-Falcon) and then incubated overnight at 37°C in a 5% CO_2/95% air mixture in a cell culture incubator (Forma Scientific, Marietta, OH). Cell culture medium was DMEM/F12 with 10% heat-inactivated calf serum plus antibiotics (Invitrogen). Test compounds were added to a final test concentration of 1 mM in the culture medium. The plate was then exposed to the stipulated LED arrays for 0, 1, 2, or 4 hours. The following day, SYTOX Green (S7020; Invitrogen-Molecular Probes) was added to the cell culture medium to a final concentration of 5 μM. A quantitative imaging platform was used in this cytotoxicity assay. This platform has been described in part (Butler MC, et al. *IOVS* 2007;48: ARVO E-Abstract 4608; Butler MC, et al. *IOVS* 2008;49:ARVO E-Abstract 5342). The plates were imaged with an epifluorescence microscope (TE-300; Nikon, Tokyo, Japan) equipped with a mercury halogen lamp, 20× (NA 0.4) plan fluor objective lens, FITC cube, and monochrome cooled 12-bit digital CCD camera (Evolution Q*ei*; Media Cybernetics, Silver Spring, MD). The SYTOX Green images were obtained with a 20-ms exposure. The images were recorded, statistically segmented, and quantified by using identical parameters throughout. The data were plotted with total fluorescence emission (523 nm) from the SYTOX Green versus time-exposed to the LED array for each of the various compounds and control agents. Data were analyzed (IP-Laboratories software, ver. 3.7; Scanalytics, Inc, Rockville, MD) and the data were plotted (Origin 6.1 software; OriginLab Corp., Northampton, MA).

Cellular Phototoxicity Assay for Macromolecules

To test the ability of LED arrays to identify biological photosensitizing macromolecules that are capable of cellular phototoxicity, we chose the only known genetically encoded wavelength-specific photoactivated macromolecule, KR.[3] HEK293S cells[25] were stably transfected with the plasmid pKR (Evrogen, Moscow, Russia), so that they would constitutively express KR, in a manner previously described.[26] Single high-level expression clones were identified on the basis of uniformity of high-level fluorescence under excitation with the appropriate optical band. Stable HEK293S-KR cells were plated into 96-well, black-walled plates and incubated at 37°C in 5% CO_2 overnight in a cell culture incubator (Forma Scientific, Marietta, OH). The plates were exposed to the $LED_{575\ nm}$ array (yellow) with the intermediate ball lens array for 15 hours in the culture incubator and then allowed to recover for an additional 12 hours. SYTOX Green was then added to the culture medium to a final concentration of 5 μM. The cells were imaged for cell death, as described earlier, in the small-molecule phototoxicity assay on the quantitative imaging platform with a 20-ms exposure time. Use of the ball lens array and long exposure times were needed to promote KR phototoxicity, because of the broad spectral emission band of the yellow LED. Much of this emission was outside the excitation band of KR and hence was lost energy. To compensate, longer times were needed to deliver a sufficient dose of photons of the appropriate band to excite KR and promote cell toxicity. As an independent test, we also used an epifluorescence microscope system with a Texas red cube and 20× or 40× lenses to efficiently excite and bleach KR on a time scale of minutes.

Wavelength-specific toxicity was demonstrated for the KR protein by using the $LED_{625\ nm}$ (red) and $LED_{575\ nm}$ (yellow) arrays. Cells stably expressing KR were plated as just described into 96-well plates and exposed to either the yellow (575 nm) or the red (625 nm) LED arrays for 13 hours. Control cells were protected from exposure to light. Cells recovered for 48 hours at 37°C in the cell culture were incubated before the cell death assay conducted with SYTOX Green (5 μM), as just described, with a 20-ms exposure time. In the microscope-based hole-burning experiments with KR, the quantitative imaging platform was used with a Texas red dichroic filter cube (Butler MC, et al. *IOVS* 2007:48:ARVO E-Abstract 4608; Butler MC, et al. *IOVS* 2008;49:ARVO E-Abstract 5342).

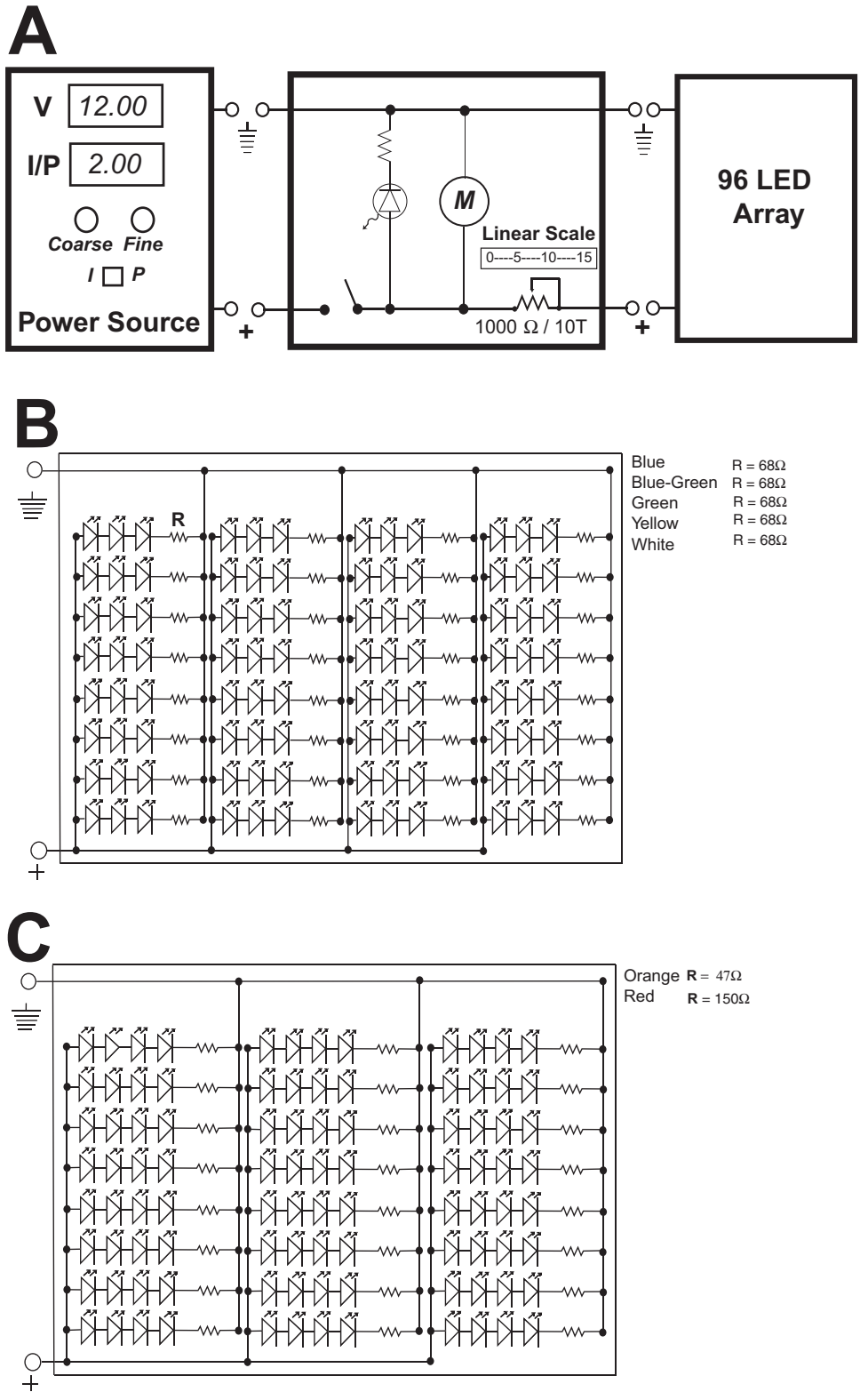

FIGURE 2. **(A)** A simplified schematic of the electronics of the LED array. The DC power supply connection is on the *left* side. A switch controls the power indicator LED, cooling motor (M), and power to the array (*right*). The variable resistor (1000 Ω) controls a large fraction of the current that can pass through the array. A simple vernier scale range knob attached to the potentiometer shaft provides repeatability of settings. (**B**) Wiring diagram for UV, blue, blue-green, green, yellow, and white arrays with three LEDs per gang. (**C**) Wiring diagram for orange and red LED arrays with four LEDs per gang.

RESULTS

LED Arrays in a Biophotonics Toolset

The LEDs chosen for construction of arrays provided a wide range of band-limited energies (Fig. 4). The LED arrays provided intense light output at maximum constant current sufficient to induce cell toxicity by two known model photoactivatable chemicals. Mean maximum intensities at different wavelengths were measured and averaged over several points immediately above the array, with a calibrated photodiode (470 nm: 4.346 ± 0.0069 mW; 502 nm: 3.066 ± 0.0064 mW; 525 nm: 3.228 ± 0.008 mW; 545 nm: 3.562 ± 0.025 mW; 575 nm: 3.969 ± 0.0067 mW; 620 nm: 1.323 ± 0.0051 mW; 625

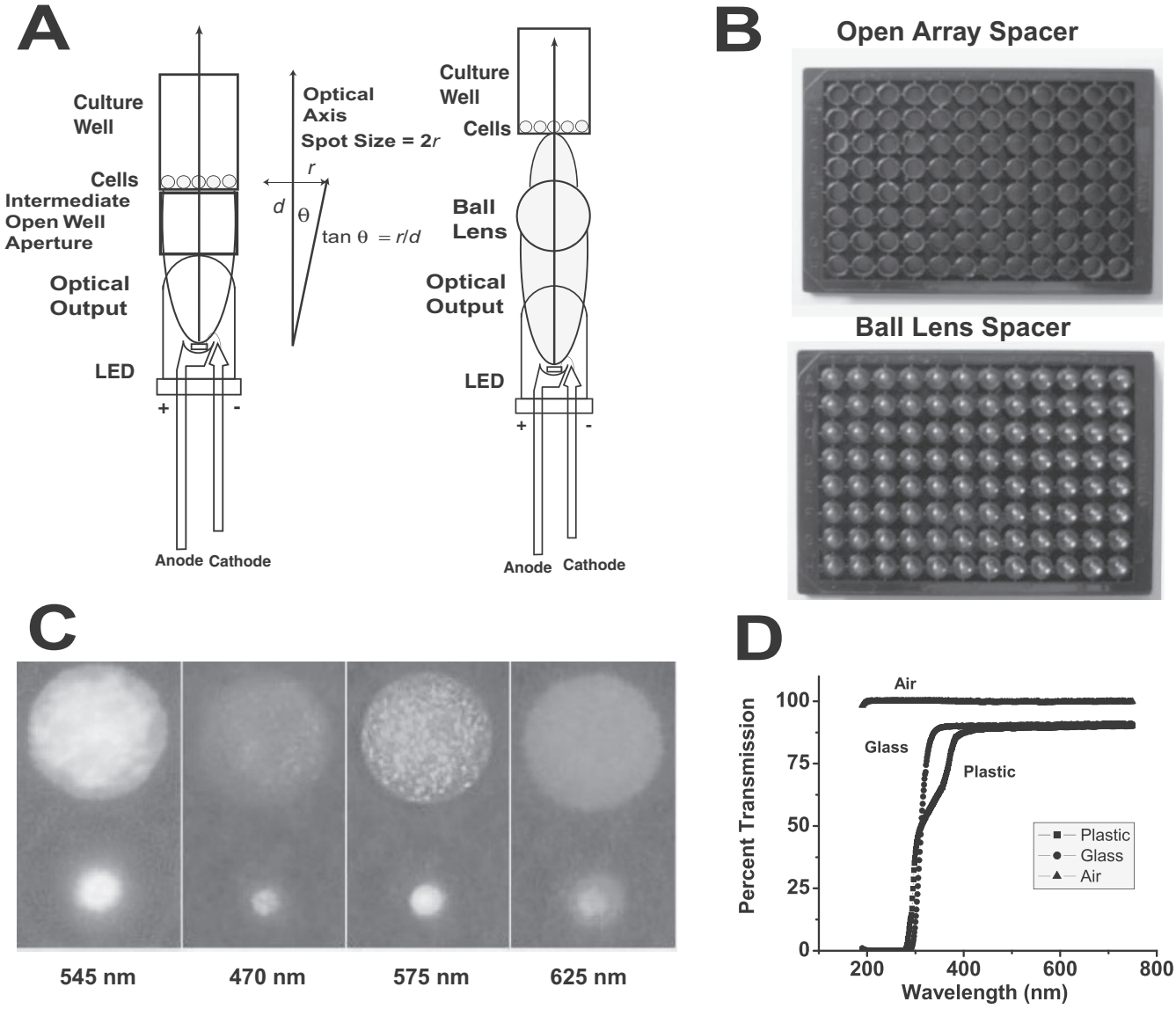

FIGURE 3. Optical properties of the LED array system. (**A**) The LED is positioned along the optical axis (perpendicular to the surface of cell growth). It has a spatial distribution of output determined by the half-angle or the FWHM. In the absence of an intermediate lens, spot size is solely determined by the half-angle of emission and the distance of the cellular array from the LED output lens. In the presence of a ball lens, the output of the LED is constrained into a tighter spot at the cellular array. (**B**) Images of an intermediate open spacer array and a spacer array loaded with acrylic ball lenses (6.35 mm diameter). (**C**) Spot sizes of the LED output in the cellular specimen plane in the absence and presence of the ball lenses for different arrays (502, 470, 575, and 625 nm) (all shown in grayscale). The top spot shows the size of the stimulus without ball lenses, which approximates the size of a well (7 mm) in a 96-well tissue culture dish. The smaller spots result from use of the ball lens array. See Table 2 for spot size dimensions. The speckled appearance of the larger spots is due to the illumination of nonuniformities in the paper used to image the spot sizes. (**D**) The optical transmission of the cell culture 96-well bottom material, either a glass or polystyrene coverslip, was measured relative to air. Glass had slightly better transmission properties below 400 nm, but both types of coverslips provided 80% transmission above 400 nm in the visible light range.

nm: 5.567 ± 0.0087 mW; and 465/570 nm: 9.673 ± 0.0153 mW; Table 1; note, full arrays were not made for 420- and 440-nm LEDs, and the amber LED at 592 was identified as a resource but never tested). These values represent the mean ± SEM when LEDs in the array were measured with the photodiode placed in a holder that isolated each LED for independent output-intensity measures. The sensor face was approximately 1 mm above the top of the LED case, which placed the tip of the clear plastic LED lens ~4 mm from the sensor face of the silicon photodiode. With the narrow beam divergence of the LEDs used in this study, the sensor face of the photodiode would be underfilled (no vignetting) by the outputs of all LEDs tested. There was a low coefficient of variation (CV = SD/mean) for the optical output of each array, which is due in part to the intrinsic low variation in outputs of LEDs as light sources, and the selection of tight-tolerance output intensity distribution bins from commercially available LED sources.

Two different power supplies were tested for their ability to stably control LED array outputs. A simple wall pack power supply provided smooth transitions in intensity between repeatable settings on the intensity potentiometer scale (change in current drive) for reliable photonic titration curves. Light output at a 12-V DC driving potential was proportional to the linear potentiometer settings until high-current drive conditions, when light output rose significantly (Supplementary Fig. S1A, online at http://www.iovs.org/cgi/content/full/51/5/2705/DC1).

TABLE 2. Optical Spot Sizes and Intensities from LED Arrays

Peak Wave-length (nm)	Mean Array Intensity (mW)	Intrinsic Spot Size Diam (mm)/ Area (mm^2)	Spot Intensity (mW/ cm^2)	Spot Size w/ Ball Lenses Diam (mm)/ Area (mm^2)	*x*-Fold Increase in Light Dose Due to Ball Lenses	Spot Intensity w/Ball Lens (mW/cm^2)
470 (blue)	6.575	5.94 (27.7)	23.7	1.43 (1.6)	17.3	410.9
502 (blue-green)	5.295	6.02 (28.5)	18.6	1.50 (1.8)	16.1	294.2
525 (green)	6.07	6.19 (30.1)	20.1	2.39 (4.5)	6.7	134.9
545 (green-yellow)	7.124	5.77 (26.1)	27.3	1.43 (1.6)	16.3	445.2
575 (yellow)	8.610	5.85 (26.9)	32.0	1.46 (1.7)	16.1	506.5
620 (orange)	3.180	6.27 (30.9)	10.2	2.01 (3.2)	9.7	99.4
625 (red)	13.610	6.27 (30.9)	44.1	2.31 (4.2)	7.4	324.1
465/570 (white)*	10.40_{465}	6.10 (29.2)	35.6	1.65 (2.1)	13.7	495.2
	5.64_{570}	6.10 (29.2)	19.3	1.65 (2.1)	13.7	268.6

From the spot sizes in the specimen plane without spacer or ball lens arrays or with the ball lens array the spot intensities were calculated after correction for silicon diode spectral sensitivity of the mean raw LED outputs (from Table 1). Mean array intensities were calculated using the mean values in Table 1 and dividing by the spectral correction factor. Spectral correction factors (calibrated) for the 400S photodiode head (EG&G UV-270BQ) are 0.676 (465 nm), 0.671 (470 nm), 0.579 (502 nm), 0.532 (525 nm), 0.500 (545 nm), 0.468 (570 nm), 0.461 (575 nm), 0.416 (620 nm), and 0.409 (625 nm).

* The relative spectral outputs of the two peaks of the white LED are 1.0 and 0.375 at 465 nm and 570 nm, respectively. We assumed that the relative distribution of the total raw output was 0.727 and 0.273, respectively at the two peak outputs. Spot intensities were determined by dividing the mean corrected array intensities by the area of the spot size.

This result was probably due to poor DC voltage regulation by this inexpensive supply. A homemade constant-voltage or constant-current (or constant wattage) linear power supply designed to control quartz tungsten halogen lamps provided a linear output over a range of practical voltages that are useful to drive LED arrays. Under constant-current conditions (1 A), increases in driving force from a 10- to 15-V led to proportional increases in light emission until the array output began to saturate (hyperbolic) (Supplementary Fig. S1B). Similarly, at a constant driving force above V_f (12 V), increases in current (0.5–2 amp) drove proportional increases in light output up to saturation (hyperbolic; Supplementary Fig. S1C). With such tightly regulated DC power supplies at a fixed setting, the output of a representative array over time (8 hours) was effectively constant (Supplementary Fig. S1D).

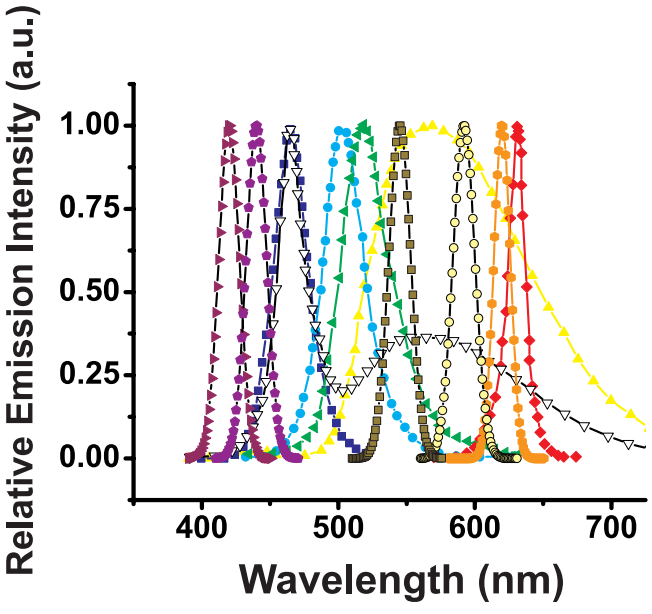

FIGURE 4. Spectral distribution of selected LEDs used in the arrays. Spectral emission data from the manufacturers is presented for 420 (*violet right triangle*), 440 (*purple pentagon*), 470 (*blue square*), 502 (*cyan circle*), 525 (*green left triangle*), 545 (*olive square with black outline*), 575 (*yellow up triangle*), 592 (*tan circle with black edge*), 620 (*orange hexagon*), and 625 nm (*red diamond*), and white emission (*white down triangle with black outline*). In several cases, spectral data were not available from the manufacturer and were simulated with a Gaussian non–linear curve-fitting function with peak base at 0, peak height at 1 (all spectra data reported are normalized), and with spectral width and peak wavelength as stipulated in Table 1.

The LEDs that were chosen from available manufacturers had outputs with high intensity and low variance, with the intent of achieving uniform array outputs. As light sources for biomedical experimentation, LEDs have low noise compared with other commonly used sources (e.g., mercury or xenon arc lamps, DC halogen lamps). The uniformity of the diode-to-diode optical output of the 96-LED arrays were measured by using a calibrated photodiode placed immediately above each LED diode in the array. The mean intensity was uniform across the two-dimensional array, regardless of the position of the LED for all full 96-LED arrays generated (Fig. 5). The selection of narrow-variance LEDs with high output guaranteed uniformity of array output. In some arrays, there were discrete LEDs with mean intensity that were statistical outliers. Through quantitative measurement of the mean outputs of each LED across the array, one could determine which LEDs should be replaced. For example, in the red (625 nm) array, there were two gangs of four LEDs that were compromised and had lower intensity. These could be replaced to assure uniformity.

The DC fan in the device maintained cooling at the level of the LEDs such that on exposure of cells to just the LED emission there was no intrinsic light-induced toxicity, even at maximum intensity (data not shown) and even though there was a slight increase in temperature (2–3°C) when the array was operated at room temperature (~20°C) or in the cell culture incubator (37°C) (Supplementary Fig. S2, http://www.iovs.org/cgi/content/full/51/5/2705/DC1). As shown in the subsequent figures (Figs. 6, 7, 8), exposure of cells to light and temperature did not promote toxicity in the absence of a small- or large-molecule photosensitizing agent. We sustained one array failure at high current densities due to catastrophic overheating during an overnight run when it was driven by the linear power source but with the fan accidentally disconnected. Hence, cooling was essential. We did not attempt further efforts to cool the arrays in this study, although it is technologically feasible, for example, with a higher power fan or a Peltier-cooled, machined, aluminum LED array block.

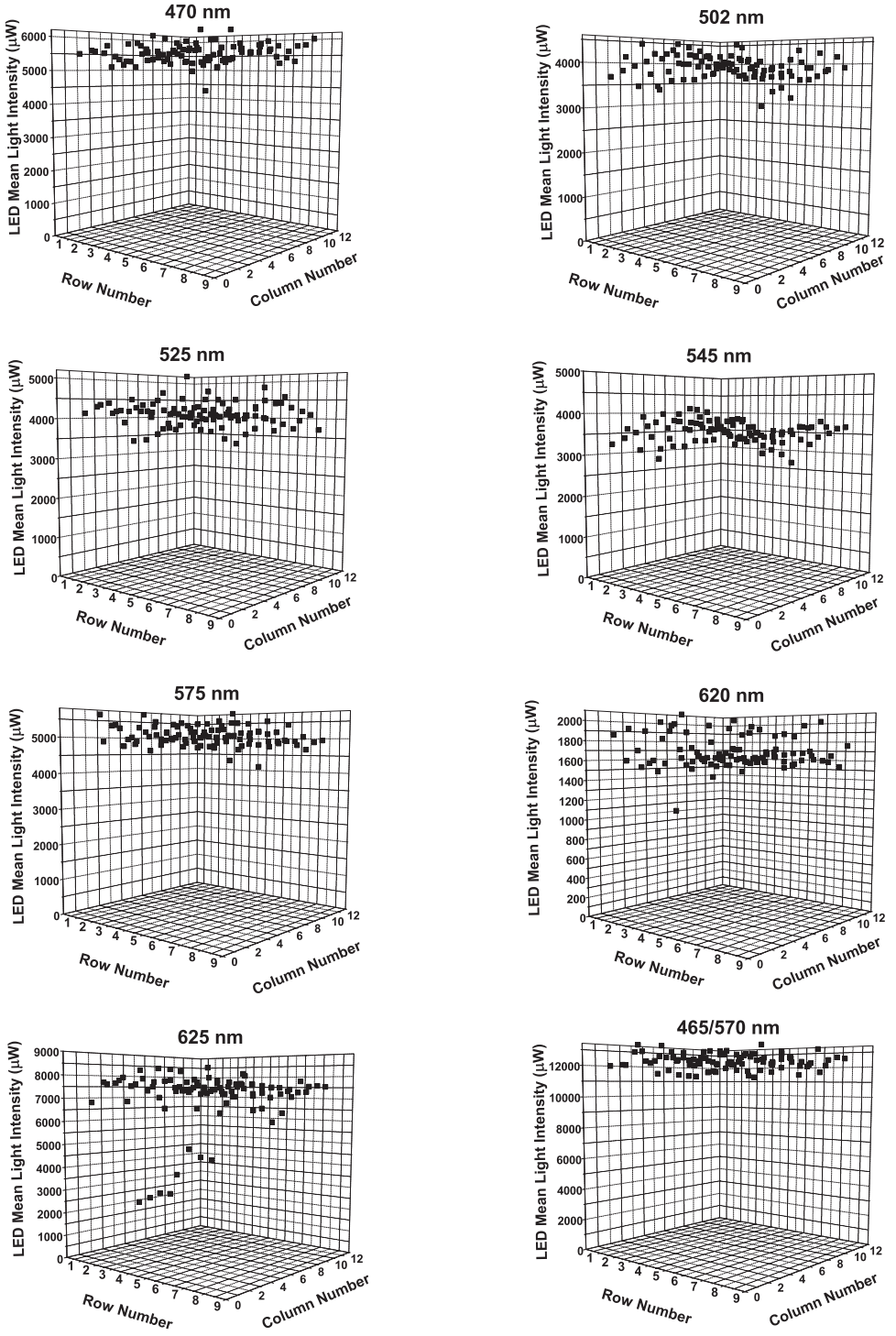

FIGURE 5. Uniform light output from 96-LED arrays. The mean light intensity over each of the 96 LEDs in all the fully assembled arrays was measured and plotted on three-dimensional diagrams. Intensity was uniform over the two-dimensional surface of all arrays. Uniformity arose due to the quality of the LEDs used in the array and the use of LED holders to position the LEDs in the array precisely, with little variance between any positions on the array. There were occasional discrete LED outliers, which could be replaced for consistent uniformity. The voltage was 12 V DC and output current varied depending on array: LED_{470nm}: 0.95 A (11.9 W), $LED_{502\ nm}$: 0.99 A (12.1 W), $LED_{525\ nm}$: 0.86 A (10.3 W), $LED_{575\ nm}$: 0.37 A (4.7 W), $LED_{620\ nn}$: 1.82 A (21.5 W), and $LED_{625\ nm}$: 0.63 A (7.7 W). The yellow array was initially tested with only 24 LEDs present, hence the lower current.

Screening Small Model Molecules for Phototoxic Induction of Cell Death

With the satisfaction of the design intent to achieve 96-well LED arrays with uniform and consistent intensity output, we hypothesized that they could be used with cultured cell arrays to test multiple compounds for phototoxicity properties. To test the utility of the LED arrays, we selected chemicals such as TMR, TMRs, and MG with optically active properties and tested them for induction of phototoxicity in cultured HEK293S cells with all the test substances at 1 μM final concentration.[2] The chemical structures of these photoactive molecules are shown (Fig. 6A). The excitation spectra of these chemicals relative to the spectral outputs of the $LED_{470\ nm}$, $LED_{525\ nm}$, and $LED_{630\ nm}$ arrays are also shown (Fig. 6B). Only the TMR and TMRs spectra had substantial overlap with the $LED_{526\ nm}$ array output and some overlap with the $LED_{470\ nm}$ array, whereas MG had a peak excitation at $\sim$ 630 nm, a wavelength at which there was essentially no output from these LED arrays. Instead, the MG absorption overlapped strongly with the $LED_{630\ nm}$ output. Cells in 96-well dishes were mixed with the candidate agents dissolved in neat DMSO and incubated at 37°C for 30 minutes in the cell culture incubator. The plates were then exposed in the 96-green-LED array for different

times at room temperature (~20°C). After the exposure, the plates were put back into the 37°C culture incubator for overnight recovery. The following day, SYTOX Green (5 μM final concentration) was added to each well. An HTS assay for cell toxicity was then conducted on a separate HTS instrument, an epifluorescence microscope equipped with a mercury vapor lamp, different dichroic cubes, and a 12-bit CCD-cooled camera. The SYTOX Green enters apoptotic cells because of compromised plasma membrane permeability and then enters the nucleus, whereupon it binds to DNA and becomes brightly fluorescent. It is selectively excluded from viable cells and is essentially nonfluorescent in the absence of bound DNA. None of the compounds tested exhibited any significant toxicity in the absence of light. Exposure to the green $LED_{525\ nm}$ array induced toxicity of both the TMR and TMRs, but not MG, in a time-dependent manner (Fig. 6C). There was significant death of cells exposed to TMR at the 2- and 4-hour exposure periods (ANOVA; $P = 0.011$ and $P = 0.000$, respectively), but no significant death after a 1-hour exposure. There was significant death of cells exposed to TMRs during the 1-, 2-, and 4-hour light-exposure periods (ANOVA, $P = 0.013$, $P = 0.000$, and $P = 0.007$, respectively). As expected, no significant phototoxicity of MG was demonstrated, even after 4 hours of exposure to green (525 nm) light. The DMSO (chemical solvent; 0.2% vol/vol) control had minimal if any toxicity associated with light exposure, and all the dark controls similarly showed no significant toxicity. Representative images of cell monolayers exposed to the chosen chemicals in the dark and after 2 hours of 525-nm green light exposures are shown (Fig. 6D). The cells were confluent in all dark control wells. The cells exposed to light and to DMSO and MG controls did not show noticeable death. Cellular toxicity, noted as loss of cells from the monolayer, occurred only in the TMR and TMRs samples. When cells treated with TMRs or MG (1 μM) were exposed to blue (470 nm), green (525 nm), or red (630 nm) LED arrays, only the green and blue arrays promoted TMRs-mediated cell death, whereas none of the arrays generated MG-mediated cell death (Fig. 6E). Similar behavior occurred at 500 nM of probe treatment (data not shown).

With a criterion exposure time of 2 hours in an 8-hour workday, a single 96-LED array could be used to screen approximately 375 compounds per day, provided that a separate device is available to measure phototoxicity by SYTOX Green nuclear DNA binding. Multiple arrays of a single LED color or an array of LED arrays representing different regions of the available LED spectrum could be used for phototoxicity screening of large libraries of small molecules.

The effects of both light and chemical dose on phototoxicity were obtained with the LED arrays. Exposure of cells to TMR at 1 μM and challenge with 525-nm light at maximum intensity on the green LED array demonstrated a linear increase in manifest cell death from 0 to 3 hours of exposure (Fig. 7A). A dose–response examination of TMR toxicity was also conducted with the 525-nm LED array with the output at maximum intensity (Fig. 7B). There was a plateau of cell death present from 0 to 200 nM TMR, which represented the baseline fraction of cells dying in the medium. At higher than 200 nM, there was an S-shaped phototoxicity titration with an LD_{50} of approximately 500 nM.

Identifying a Genetically Encoded Biomolecule with Photosensitizing Properties

The KR protein is a genetically encoded fluorescent photosensitizer molecule that is capable of generating $^1O_2$ after exposure to green-yellow light (KR has 585-nm peak absorption, 610-nm peak emission).[3] HEK293S cells stably expressing KR fluorescent protein were used to begin to assess this genetically encoded phototoxicity agent. Exposure to the $LED_{575\ nm}$ (yellow) array led to bleaching of the KR fluorescence, as imaged with a fluorescence microscope and a Texas red cube (Fig. 8A, left). SYTOX Green staining for toxicity showed that the only HEK293S cells dying in the wells were those expressing KR and exposed to the yellow LED array (with intermediate ball lenses) at maximum intensity for 15 hours (Fig. 8A, right). Naïve HEK293S cells that did not express KR demonstrated background cell death that was not different between no and full exposure to yellow light. Quantitative assessment of the spectral properties of KR-mediated cellular death is shown (Fig. 8B). HEK293S cells expressing KR did not show any increased phototoxicity when exposed to the red LED array when compared to the unexposed (dark) control, whereas KR-expressing cells exposed to the yellow LED array showed abundant and statistically significant cell death. The impact of these treatments on cellular monolayers was assessed on the epifluorescence microscope equipped with FITC (SYTOX Green) and Texas red (KR) fluorescence cubes (Fig. 8C). KR expressing HEK293S cells were not exposed to light (row A), exposed to the yellow $LED_{575\ nm}$ array (row B), or exposed to the red $LED_{630\ nm}$ array (row C). Red light (630 nm) did not activate KR. Bright-field images of the cells are shown in the first column. KR fluorescence images showed the effect of bleaching with the yellow but not the red light. SYTOX Green labeling showed cell death only in the area of KR bleaching by yellow light. The merged images of KR and SYTOX Green precisely demonstrate that the area of cells in wells where KR was bleached (to generate $^1O_2$) were the only regions that manifested high-density cell death. The nature of the spatial hole-burning that was performed on the LED array with relatively crude ball lenses did not portray the refined spatial control over KR bleaching that can be achieved. On the epifluorescence microscope a monolayer of KR-expressing HEK293S cells was exposed to an intense spot of green light (excitation filter: peak 535 nm, FWHM 25 nm, 10.76 W/cm^2) generated by 20× and 40× (40× not shown) objective lenses and a Texas red cube (Fig. 8D). These lenses created spot sizes in the specimen plane of approximately 500 or 250 μm, respectively. Note the crisp circle of KR bleaching that was obtained with these spots of light (Fig. 8Da) and the subsequent localization of cell death that resulted from this stimulus, noted at 2 days after exposure (Fig. 8Db). By the third day after exposure, many dead cells had cleared the area of KR bleaching, as noted both by SYTOX Green (Fig. 8Dc) and bright-field imaging (Fig. 8Dd).

Discussion

A Novel Biophotonics Instrument as a Modular Component to HTS and HCS Platforms

With the current photonics device, we sought to demonstrate the potential use of this technology for HTS but did not screen a large combinatorial library. We describe 96-well LED arrays formulated from sets of 5-mm diameter commercially available discrete optoelectronic elements that were stably placed and electronically wired into preformed 96-well cell culture plate arrays. A broad range of LEDs covering much of the visible spectrum were placed into arrays. Near-UV or near-infrared LED arrays are also feasible. These LEDs have high-intensity output, narrow spatial distribution bands, and tight intensity-distribution manufacturing tolerances. The current instrument was starkly simple in electronic and optical design but was sufficient to demonstrate proof-of-principle functionality. Statistically significant mammalian cell death was demonstrated after cells incubated with small molecules were exposed to optical energy of appropriate bandwidth. TMR and structurally

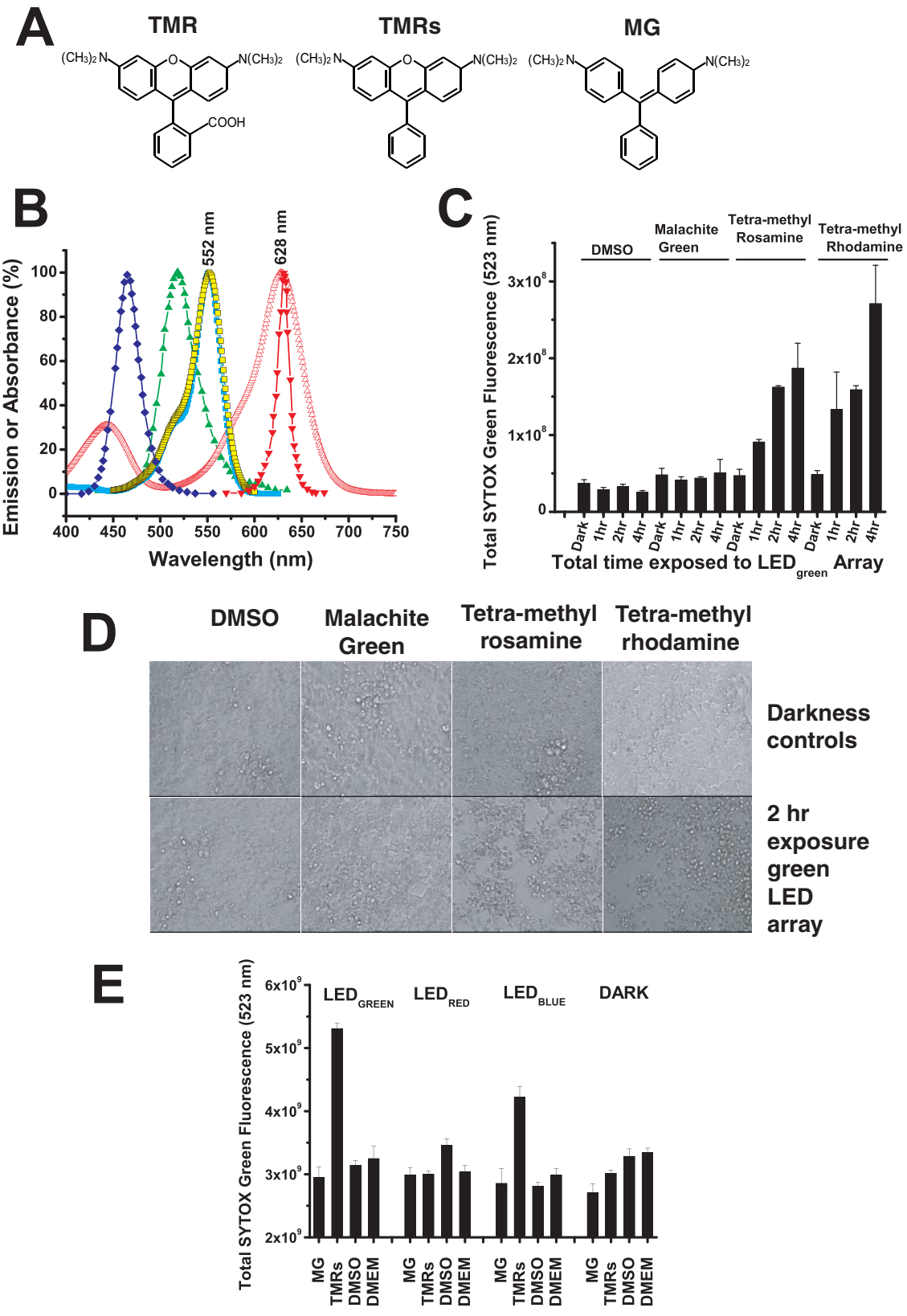
A
TMR
TMRs
MG
(CH3)2N
N(CH3)2
COOH
B
552 nm
628 nm
Emission or Absorbance (%)
Wavelength (nm)
C
DMSO
Malachite Green
Tetra-methyl Rosamine
Tetra-methyl Rhodamine
Total SYTOX Green Fluorescence (523 nm)
Dark
1hr
2hr
4hr
Total time exposed to LED green Array
D
DMSO
Malachite Green
Tetra-methyl rosamine
Tetra-methyl rhodamine
Darkness controls
2 hr exposure green LED array
E
LED GREEN
LED RED
LED BLUE
DARK
Total SYTOX Green Fluorescence (523 nm)
MG
TMRs
DMSO
DMEM

related TMRs in micromolar concentrations were capable of eliciting cell death after exposure to 525 nm optical energy overlapping the major absorption dipole of these small molecules. In contrast, structurally related MG, which is not optically active in on green excitation, did not cause cell death. The genetically encoded KR fluorescent protein promoted highly circumscribed death in cell monolayers on absorption of light that promotes fluorescence and $^1O_2$ formation during photobleaching. In summary, a proof-of-principle demonstration was made of the capacity of the LED arrays to induce cell death by a small, representative set of optically active small molecules (TMR, TMRs, and MG) and a novel optically active biomolecule (KR).

The LEDs used to make the arrays were chosen because they have robust output wattages, narrow beam diameters, and low tolerances on maximum output. The optical output of the arrays exhibited uniform intensity across the two-dimensional culture surface such that each well in a 96-well culture plate achieved a comparable number of photons over arbitrary exposure durations. The use of cell culture plates to form the LED and spacer arrays (open, ball lens) guaranteed registry of the stacked LEDs, the intermediate spacer plates, and the cell culture well arrays along each of the 96 parallel optical axes. The ball lenses were able to concentrate light into the center of the 7-mm culture wells. Although the optical stimulus to a single population of cells in a well was nonuniform in this case, we found that statistically significant toxicity was still measurable. The LED arrays were used in concert with a separate HTS-imaging platform on which cytotoxicity measures were obtained (see the Methods section). A fluorescent plate reader with optics tuned to measure the SYTOX Green fluorescence could also be used. There are other fluorescent dyes capable of detecting and quantifying cell death (e.g., SYTOX Blue, SYTOX Orange, ethidium homodimer-1, and dimeric and monomeric cyanine dyes). The combination of the LED arrays and the quantitative HTS-imaging platform allowed screening of chemical libraries for novel PDT candidate agents. In addition to screening under fixed-parameter criterion conditions (e.g., 2-hour exposure, maximum intensity) the system also allowed for dose- and time-dependent toxicity measures, to fully characterize optimum leads. When libraries of agents are tested across multiple LED arrays, this instrument can facilitate identifying lead compounds that exhibit wavelength-specific toxicity.

All the LED arrays were designed for use with a single power supply and control box with a simple manual rheostat modulator to control array LED current and optical output. Cell culture preparations and SYTOX Green phototoxicity assays were all conducted by manual pipetting and manipulation. Advances could be made to the array and control electro-optics to facilitate HTS (Supplementary Table S1, http://www.iovs.org/cgi/content/full/51/5/2705/DC1). For example, a larger control box is feasible with a tightly regulated DC power supply and sufficient amperage drive for up to 10 LED arrays (manufactured from a wide range of available LEDs, e.g., Table 1) covering a broad spectral range. LEDs are intrinsically low-noise optical devices and certainly offer much quieter performance than tungsten halogen or arc lamps.[27] LED technology is modular and inexpensive, such that arrays covering finer ranges of wavelengths and intensities are immediately feasible. A choice of arrays could be made on the basis of different classes of chemistry in small-molecule chemical libraries. The arrays could also be used in screens of combinatorial fluorescent protein libraries, to identify discrete fluorescent proteins with desired optical properties that are improved photosensitizing agents. Individual arrays could be equipped with silicon photodiodes, to measure a fraction of array output as a feedback signal to regulate current drive, such that the photon (or

FIGURE 6. Small-molecule phototoxicity elicited by LED arrays. (**A**) Chemical structures of TMR, TMRs, and MG. (**B**) The absorption (excitation) spectra of TMR (peak 552 nm), TMRs (peak 552 nm), and MG (peak 628 nm) are shown relative to the spectral output of the $LED_{470\ nm}$ blue array (peak 465 nm), the $LED_{525\ nm}$ green array (peak 518 nm), and the $LED_{625\ nm}$ red array (peak 631 nm). The absorption spectra of TMR and TMRs overlap with the optical stimulus spectra of the LED green array and in part with the LED blue array, indicating that these arrays have the potential to induce phototoxicity from TMR and TMRs, but not from MG. (**C**) SYTOX Green cytotoxicity assay after exposure of cells to TMR, TMRs, or MG (all at 1 μM) followed by exposure to the highest intensity of the green $LED_{525\ nm}$ array for 1, 2, or 4 hours. Increases in the SYTOX Green fluorescence indicates increased cell death. The DMSO control (at 0.2%; vol/vol) has the solvent at the same concentration delivered into the cell culture media for the three test chemicals. Dark controls were not illuminated with LED light. ANOVA of all the samples led to the outcome that the means were not the same ($F = 13.12$, $P = 1.17E\text{-}9$). ANOVA tests run over the four sets of the chemical test substances found that the means were not different for the various test conditions for DMSO ($F = 2.12$, $P = 0.18$), or MG ($F = 0.154$, $P = 0.92$), but they were different for the various test conditions for TMRs ($F = 14.87$, $P = 0.001$) and TMR ($F = 6.91$, P = 0.01). These data suggest that TMRs and TMR are both photoactive chemicals that promote cellular apoptosis under the conditions of light exposure. Further statistical testing was performed on this hypothesis by comparing all samples of the different chemicals in the same condition (dark and 1, 2, and 4 hours of light exposure). ANOVA of all the dark samples found no differences among the sample means ($F = 0.62$, $P = 0.62$). ANOVA on all the 1-hour samples also found no difference among the sample means, although the probability was close to statistical criterion level ($\alpha = 0.05$) ($F = 3.86$, $P = 0.06$), most likely due to the TMRs and TMR samples at the 1-hour exposure. ANOVA of the 2- and 4 hour samples found strong differences between the sample means (2 hour: $F = 453.41$, $P = 2.87E\text{-}9$; 4-hour: $F = 14.04$, $P = 0.001$). The progress of the statistical analysis suggested that the TMRs and TMR both induced cellular phototoxicity at both the 2- and 4-hour doses of light. The TMRs and TMR samples at 2 and 4 hours were then both tested (*t*-test) relative to their dark controls (TMRs: 2 hours [$t = 13.80$, $P = 1.60E\text{-}4$] and 4 hours [$t = 4.22$, $P = 0.01$] versus dark control; TMR: 2 hours [$t = 14.75$, $P = 1.23E\text{-}4$] and 4 hours [$t = 4.45$, $P = 0.01$] versus dark control), and the results showed that both TMRs and TMR promote cellular phototoxicity over a 1- to 4-hour period when exposed to light with energy overlapping the absorption dipole of these agents. (**D**) Representative microscopic cell culture images (phase contrast) of samples from TMR, TMRs, MG, and DMSO control cultures that were kept in the dark (*top row*) versus samples that were exposed to the $LED_{525\ nm}$ green array at maximum intensity for 2 hours (*bottom row*). Only the cells that received TMR or TMRs and light of the appropriate wavelength exhibited cytotoxicity. (**E**) Toxicities of TMRs and MG were measured on the blue (470 nm), green (525 nm), and red (625 nm) LED arrays after 2-hour exposures followed by SYTOX Green staining. ANOVA was performed on all data sample sets for each LED array and the darkness control. The means were found to be significantly different for the green ($F = 62.89$, $P = 1.31E\text{-}7$), red ($F = 5.71$, $P = 0.01$), and blue ($F = 18.43$, $P = 8.69E\text{-}5$) LED arrays and, surprisingly, for the darkness control ($F = 8.34$, $P = 0.003$). With DMSO used as the pertinent sample, control *t*-tests were performed to compare means within sample sets from the LED arrays and darkness control. On the green LED array MG did not show significant toxicity ($t = 1.07$, $P = 0.32$), whereas TMRs showed significant toxicity ($t = -19.00$, $P = 1.37E\text{-}6$) compared with DMSO. On the red LED array both MG and TMRs show significant difference in toxicity compared with DMSO, but both induced mean toxicities that were lower than the control (MG versus DMSO: $t = 3.04$, $P = 0.0227$; TMRs versus DMSO: $t = 3.97$, $P = 0.0074$), and there was no significant difference between MG and TMRs ($t = 0.067$, $P = 0.95$). On the blue LED array MG showed no significant toxicity relative to DMSO ($t = 0.1884$, $P = 0.86$), whereas TMRs showed significant toxicity relative to DMSO ($t = -7.76$, $P = 2.40E\text{-}4$) and MG ($t = 4.69$, $P = 0.003$). In the darkness control MG showed a lower mean value than DMSO control ($t = 3.18$, $P = 0.02$), but the TMRs versus DMSO ($t = 2.06$, $P = 0.085$) and the TMRs versus MG ($t = 2.10$, $P = 0.08$) showed no differences. In summary, there was significant toxicity of TMRs on both the $LED_{525\ nm}$ and $LED_{470\ nm}$ arrays, but not the $LED_{625\ nm}$ red array. MG showed no significant toxicity on any of the LED arrays. To power the $LED_{470\ nm}$ array, a constant voltage of 12 V DC and output current 1.0 A (12 W) was used; for the $LED_{525\ nm}$ array, a constant voltage of 12 V DC and output current 0.80 A (9.8 W); and for the $LED_{625\ nm}$ array, a constant voltage of 12 V DC and output current of 0.63 A (7.6 W) was used.

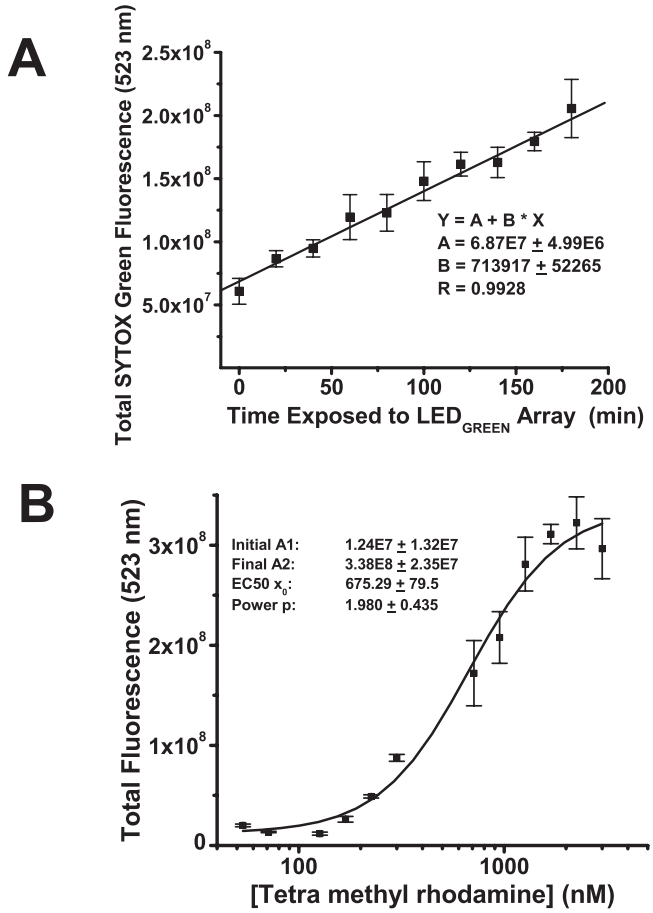

FIGURE 7. Light dose–response and chemical ligand dose–response in a phototoxic condition. (**A**) With TMR at 1 μM the $LED_{526\ nm}$ green array at maximum intensity (12 V DC, 1.5A) was used to stimulate cells for 0 to 3 hours before the SYTOX Green cytotoxicity assay. There was a linear response of cell death to a 525-nm photon dose ($R = 0.9928$, $P < 0.0001$). (**B**) With the 525-nm LED array at a 2-hour exposure, the TMR ligand concentration was varied from 0 to 1000 nM. A SYTOX Green assay was performed 24 hours later. The dose–response curve had the characteristic nonlinear appearance and was fit with a Boltzmann function. The LD_{50} for TMR is 675 ± 80 nM as determined from a logistic curve fit to the dataset $[y = (A_1 - A_2)/(1 + x/x_0)^p + A_2]$, where A_1 is the minimum y value, A_2 is the maximum y value, x_0 is the LD_{50}, and p is the power, $p \sim 2$. SYTOX Green assay data were collected with a 20-ms exposure.

energy) flux/well across arrays of different color are uniform. This method would allow library screening to occur under conditions of equal photons or equal energy at different wavelengths. Better cooling strategies could be used to reduce the small steady state temperature rise that does occur but appears not to induce toxicity. Computer control on output intensity and temporal output (constant, flash) could be designed through appropriate digital-to-analog interfaces. Robotic tools for plating cells, moving culture plate arrays onto and off of the HTS LED platform, micropipetting fluorescent dyes, and moving plates to the other HTS device for cytotoxicity measures could also be incorporated. Finally, we expect that the design strategy is extendable to LED arrays fabricated with narrow-beam, 3-mm LEDs, which could be used in 384-well cell culture arrays, to increase the number of samples processed in a given day.

During preparation of this manuscript we became aware of a single-wavelength LED array used to evaluate agents for bacterial chemotherapy.[28] In that study, there was no attempt to integrate the geometry of the LED array into a cell culture array. In fact, a 52-LED array (671 nm) was used with 12-well culture dishes, which is not a format for HTS. The current device is novel, in that the LED arrays are integrated with the geometry of the 96-well cell culture arrays for HTS and HCS and can be extended to even higher density culture and LED arrays.

Scientific Issues for HTS and HCS for Novel Photosensitizing Agents

The contemporary model of drug discovery has the following steps: (1) target validation, (2) lead candidate identification, (3) lead candidate optimization, (4) preclinical testing in appropriate animal models, and (5) FDA-approved human clinical trials. Target validation is the process of proving the relevance of a specific molecular target for therapy. This issue is a complex one for PDT, as plasma membrane, mitochondrial membrane, and lysosomal membrane components as well as signaling pathways can be involved with different agents.[1–3,29] The biophotonics instrument described herein can play a major role in photosensitizer drug discovery in the areas of novel lead identification and optimization.

HTS of rich combinatorial libraries for lead candidates is more readily managed in easy-to-use cell culture systems with appropriate formats (e.g., 96-, 384-well). Photosensitization and phototoxicity are properties at the interface of the chem-

FIGURE 8. Wavelength-specific toxicity of Killer Red. (**A**) The fluorescence of KR in HEK293S cells before and after peak 575-nm illumination is shown, demonstrating the bleaching effect of light from the $LED_{575\ nm}$ yellow array for 15 hours (*left*). There was a strong significant decrease of KR fluorescence after exposure to yellow light ($t = -22.29$, $P = 5.34E\text{-}7$). The SYTOX Green fluorescence was measured 15 hours after light exposure. The assay measured significant cell toxicity only in HEK293S cells expressing KR that were exposed to the $LED_{575\ nm}$ array. ANOVA was used to compare sample means for KR expressing and control 293S cells kept in dark or exposed to yellow light (*right*). The means for cell death were significantly different among these samples ($F = 18.87$, $P = 7.73E\text{-}5$). *t*-Tests were used to compare yellow light–exposed, KR-expressing samples versus the dark control ($t = 5.44$, $P = 0.002$) and naïve HEK293S cells exposed to yellow light versus dark controls ($t = -0.632$, $P = 0.55$). Bleaching of KR by yellow light clearly promoted enhanced phototoxicity of HEK293S cells, but exposure to the same dose of light had no impact on naïve HEK293S cells. (**B**) KR-mediated phototoxicity was wavelength dependent. At more than 13 hours' exposure, the 575-nm but not the 625-nm array promoted cell death in HEK293S cells expressing KR, whereas the dark control show no cell death. The SYTOX Green assay was conducted 48 hours after exposure to light. ANOVA was conducted, and the sample means were found to be significantly different ($F = 22.19$, $P = 1.17E\text{-}7$). There was no significant difference measured between the HEK293S cells expressing KR exposed to $LED_{625\ nm}$ and the dark control ($t = -0.110$, $P = 0.913$). However, there was a significant difference between the dark control and the yellow LED array–exposed cells ($t = -4.39$, $P = 1.15E\text{-}4$) and between the yellow– and red LED array–exposed cells ($t = 5.197$, $P = 7.16E\text{-}6$). (**C**) Representative images of the cells under bright-field, KR epifluorescence, SYTOX epifluorescence, and merged. The cells expressing pKillerRed plasmid that were not exposed to light (**Ca–d**) or were exposed to the $LED_{625\ nm}$ (**Ce–h**) or the $LED_{575\ nm}$ (**Ci–l**) array for 13 hours with ball lenses in the intermediate spacer plate. SYTOX Green was added to each well to a final concentration of 5 μM. (**D**) Monolayers of KR expressing HEK293S cells were placed in culture wells on an epifluorescence microscope stage. A 20× lens was used to deliver green-yellow light to the cells through a Texas red filter cube for a period of 1 hour. The excitation light intensity at peak 535 nm (FWHM 25 nm) was 10.76 W/cm^2, with the spot size of KR bleaching approximately 500 μm in diameter. (**Da**) KR bleaching showed strict spatial constraint and followed the stimulus spot size in geometry. (**Db**) The next-day SYTOX Green assay demonstrated a uniform circular patch of dead and dying cells in the area of KR bleaching. (**Dc**, **Dd**) By 3 days after stimulus, the dead cells were clearing from the area of KR bleaching (**Dc**, SYTOX Green staining; **Dd**, phase-contrast image). Essentially, all cells in the bleached area were killed.

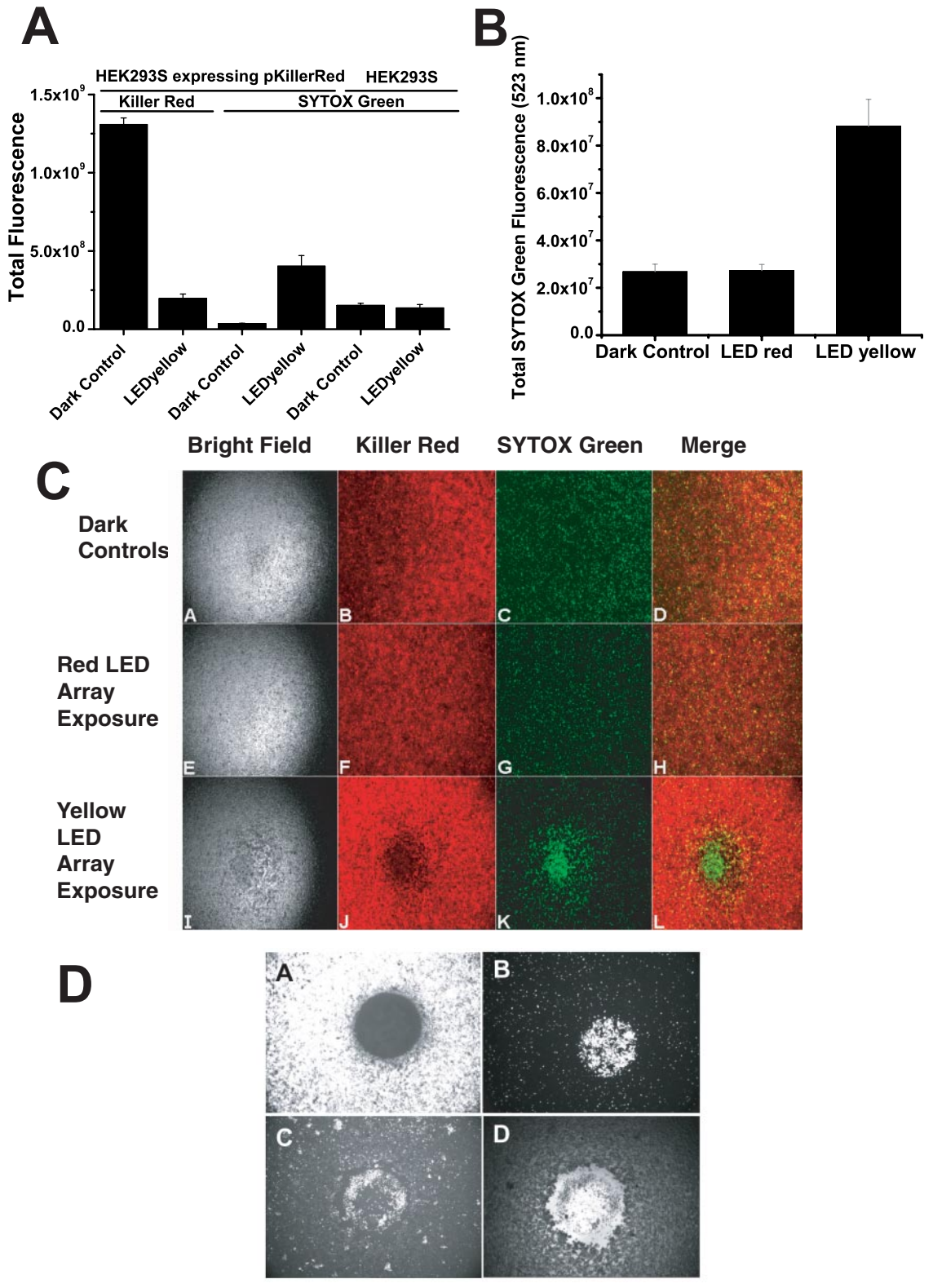
A
HEK293S expressing pKillerRed
HEK293S
Killer Red
SYTOX Green
Total Fluorescence
1.5x10^9
1.0x10^9
5.0x10^8
0.0
Dark Control
LEDyellow
Dark Control
LEDyellow
Dark Control
LEDyellow
B
Total SYTOX Green Fluorescence (523 nm)
1.0x10^8
8.0x10^7
6.0x10^7
4.0x10^7
2.0x10^7
0.0
Dark Control
LED red
LED yellow
C
Bright Field
Killer Red
SYTOX Green
Merge
Dark Controls
Red LED Array Exposure
Yellow LED Array Exposure
A
B
C
D
E
F
G
H
I
J
K
L
D
A
B
C
D

ical or macromolecular compound and cellular structure and metabolism. Small-molecule phototoxic agents, as those used in this study for proof of principle, are known to exert primary phototoxicity in cellular organelles and housekeeping metabolism that are common to *all* cell types and that reside below differentiated structural and functional hierarchy (e.g., mitochondrial energy metabolism, cellular responses to stress, and apoptosis induction).[29] Secondary repair processes emerging from primary phototoxic stress are also likely to occur within cellular housekeeping properties. One expects that most photosensitizing agents will perform similarly in a wide range of cell types.

For lead optimization, we recommend that the ultimate target cells be used to encompass as many possible cellular or tissue variables that could influence therapeutic efficacy. VECs are clearly the target cells for development of novel therapies for ocular pathologic angiogenesis. Although VECs are likely to have unique repair responses to phototoxic stress that could influence efficacy, they can be difficult to grow in culture and are certainly challenging to transfect with plasmids. These properties of VECs complicate their use in initial HTS to identify novel lead candidates. There are some immortalized cell lines that model the microvascular properties and gene expression patterns of pathologic angiogenesis.[30] These could be used for lead optimization, provided that molecular expression patterns model the VECs of pathologic angiogenesis.

The chick chorioallantoic membrane has a highly relevant physiological endpoint for testing the impact of agents on natural angiogenesis.[16] However, this model is impractical for HTS of combinatorial chemical or biological libraries. The live zebrafish embryo vascular arch model is interesting but requires access to that particular model and zebrafish culture facilities, which are not commonly available.[17] On a different level, it is unclear to what extent such nonmammalian models simulate sufficient molecular target conservation, housekeeping functions, and signal-generating capacity to provide an appropriate environment to identify or optimize agents that could be used to treat *human* pathologic angiogenesis.

In this study, we used HEK293 cells because they are easy to grow in large numbers and they transfect exceptionally well with plasmids (e.g., to test pKR). The development of the HTS instrument was not intended for HEK293 cells, but they provided a useful resource to test proof of principle that the biophotonics instrument could identify phototoxic agents. These cells have clearly served their purpose to test the instrument, but not to screen for new agents. Their utility in the experimental design was not to test specificity of potential PDT agents. Rather, it was to establish the functionality of the instrument to perform such a task.

Toward a Novel Gene Therapy Approach for Pathologic Ocular Angiogenesis

With the instrument described in this study and toward a novel gene therapy approach for ocular pathologic angiogenesis, we identified and began testing a novel photosensitizing fluorescent protein called KR. There is unique potential for a photosensitizing agent with its spectral properties[3] (585-nm peak excitation, 610-nm peak emission) and one that can be genetically expressed. KR's potential was realized with the brightest available yellow LED technology with a broadly distributed energy emission band (568 ± 61.2 nm; Fig. 4). Only a fraction (48%) of the available energy of the yellow LED emission was able to excite KR (peak 583 ± 34.5 nm) to induce fluorescence, and the measured cellular phototoxic effect required 15 hours of exposure. The total delivered photon dose is a product of irradiance (photons/mm^2/s) and duration of exposure. On the biophotonics instrument described, photon dose was modulated by condensation of optical energy with ball lenses (increased irradiance) and control of exposure time. On a microscope equipped with a mercury vapor lamp and a narrow emission filter overlapping KR excitation, it takes only minutes to bleach cellular KR and achieve highly efficient photosensitization and apoptotic cell death. Thus, KR is a particularly strong photosensitizing agent, but current yellow-band LED technology is limited. With improvement in LED materials science, we expect that the yellow and other bands will achieve narrower and brighter emissions. The HTS LED array instrument can be rapidly upgraded with improved LEDs at any time.

We propose a novel therapeutic strategy called PhotoGene Therapy (PGT) for pathologic angiogenesis of the retina, choroid, or eye. In PGT, a vector delivers the expression construct for genetically encoded KR or similar genetic cargo into the VECs of the pathologic angiogenesis of CNV or the retina, or into retinal or choroidal tumor cells. Such vectors could be viral or nanoparticle elements engineered with surface ligands that allow homing to the unique surface receptor landscape of the target VECs of pathologic angiogenesis from within the intravascular volume.[31,32]

There are many potential advantages of the therapeutic strategy of PGT with KR as the genetically encoded photosensitizer. Cellular uptake and expression of KR would optically label the VECs of the pathologic angiogenesis and allow improved optical interrogation of the location of the CNV. CNV is often difficult to diagnose by fluorescein angiography because of overlying fluid, lipid exudates, or blood that act as optical screens to block diagnostic fluor excitation or emission.[33,34] KR is excited in the yellow energy band, which is not fully absorbed by blood and is transparent through lipid exudates. And, KR emits in the red, which transmits readily through overlying heme or exudates with minimal absorption. That is, the optical properties of KR appear well suited for identifying the location of CNV amid overlying absorbing (blocking) screens. A second advantage is that mapped spatial localization of the neovascular lesion would allow focal KR bleaching with photon doses that are below toxic retinal light damage levels because of the high extinction and quantal yield of KR. A third advantage is that a genetically encoded photosensitizer allows promotion of VEC apoptosis more efficiently from within the restricted diffusional volume of the cell to enhance the probability of definitive thrombosis of the neovascular lesion and yield its involution. Similarly, in tumors, apoptotic death of activated VECs could be mediated by light. A fourth advantage of KR-mediated PGT is that the extent of treatment can be directly visualized and monitored over time by fundus fluorescence measurements. Once bleached, KR fluorescence does not reemerge from a cell until new KR protein synthesis has occurred. Surviving transduced VECs within a treated neovascular lesion would again express KR and lead to reappearance of a red fluorescent neovascular net or groups of fluorescent cells on repeated optical interrogation. Repeated treatments may be needed to fully involute CNV other pathologic angiogenic lesions or tumors in the eye.

There are also distinct challenges to realizing PGT. It is critically dependent on a successful intravascular delivery of vector into activated VECs that line pathologic angiogenesis within the retina, choroid, or eye. Viral or nanoparticle vectors with appropriate surface motifs are needed to promote molecular recognition and transduction by VECs within pathologic angiogenic vessels that maintain a flow stream. The overriding abundance of quiescent VECs in the mammalian body are not in the cell cycle. However, replicating VECs in pathologic angiogenesis has upregulated cell surface receptors (i.e., markers) that are not expressed in quiescent VECs. This property creates a potential for the design of highly selective homing

vectors with engineered surface ligands that bind to upregulated VEC surface molecular targets (e.g., integrin $\alpha_v\beta_3$ receptors[31,32]) from the intravascular side of the polarized VECs. This endeavor is a challenging one, but viral and nanoparticle homing vectors have already emerged that selectively target VECs within pathologic angiogenesis from the intravascular volume.[35–42] A potential disadvantage of the native KR photosensitizer is that its absorption band has partial overlap with the hemoglobin (Hb) absorption band. However, both the peak and the entire red edge of the native KR absorption band are sufficiently well separated from the Hb absorption band that excitation of KR in VECs of a CNV lesion could occur efficiently despite overlying Hb (modeling data not shown) (Sullivan et al. manuscript in preparation). One can also look forward to combinatorial mutagenesis to realize new far-red fluorescent proteins that preserve the phototoxic potential of KR but shift its absorption spectrum slightly to the red to completely avoid the Hb absorption dipole.[43] In addition, PGT is not intended to treat the underlying stimuli of pathologic angiogenesis (e.g., ischemia, inflammation). Rather, it is intended to suppress sequelae of pathologic angiogenesis (e.g., leakage, bleeding, and scarring). Further experimental work is clearly essential to demonstrate proof of principle of the PGT therapeutic strategy.

Conclusions

A proof-of-principle biophotonics device intended for HTS and HCS of novel photosensitizing agents was developed and demonstrated. The instrument can be used for future screening of libraries of small molecules or macromolecules to identify molecules with novel photoactive PDT or PGT properties. The same device can be used to optimize the range of optical and cellular properties of such agents. Coupled to robotic tools, these arrays have the potential to screen sizable chemical and biological molecular libraries for novel photosensitizing agents. A genetically encoded photosensitizer has been identified through the use of a biophotonics instrument that has potential for use in a proposed novel gene therapy approach to CNV and ocular pathologic angiogenesis.

Acknowledgments

The authors thank Kenneth Tramposch (Associate Vice President for Research, SUNY University at Buffalo) for support through the course of this emerging study.

References

1. Dougherty TJ, Gomer CJ, Henderson BW, et al. Photodynamic therapy. *J Natl Cancer Inst.* 1998;90:889–905.
2. Kessel D, Luo Y. Photodynamic therapy: a mitochondrial inducer of apoptosis. *Cell Death Differ.* 1999;6:28–35.
3. Bulina ME, Chudakov DM, Britanova OV, et al. A genetically encoded photosensitizer. *Nat Biotechnol.* 2006;24:95–99.
4. Miller J, Schmidt-Erfurth U, Sickenberg M, et al. Photodynamic therapy with verteporfin for choroidal neovascularization caused by age-related macular degeneration: results of a single treatment in a phase 1 and 2 study. *Arch Ophthalmol.* 1999; 117:1161–1173.
5. Treatment of age-related macular degeneration with photodynamic therapy (TAP) study group: photodynamic therapy of subfoveal choroidal neovascularization in age-related macular degeneration with verteporfin: one-year results of 2 randomized clinical trials. TAP Report 1. *Arch Ophthalmol.* 1999;117:1329–1345.
6. Bressler N. Treatment of age-related macular degeneration with photodynamic therapy (TAP) study group: photodynamic therapy of subfoveal choroidal neovascularization in related age macular degeneration with verteporfin: two year results of 2 randomized clinical trials. TAP Report 2. *Arch Ophthalmol.* 2001;119:198–207.
7. Kramer M, Miller J, Mihaud N, et al. Liposomal benzoporphyrin derivative verteporfin photodynamic therapy. *Ophthalmology.* 1996;103:427–438.
8. Klais CM, Ober MD, Freund KB, et al. Choroidal infarction following photodynamic therapy with verteporfin. *Arch Ophthalmol.* 2005;123:1149–1153.
9. Brown DM, Kaiser PK, Michels M, et al. Anchor Study Group. Ranibizumab versus verteporin for neovascular age-related macular degeneration. *New Engl J Med.* 2006;355:1432–1444.
10. Heier JS, Boyer DS, Ciulla TA, et al. Ranibizumab combined with verteporfin photodynamic therapy in neovascular age-related macular degeneration: year 1 results of the FOCUS Study. *Arch Ophthalmol.* 2006;124:1532–1542.
11. Rosenfeld PJ, Brown DM, Heier JS, et al. MARINA Study Group. Ranibizumab for neovascular age-related macular degeneration. *N Engl J Med.* 2006;355:1419–1431.
12. Bashur ZF, Schakal A, Hamam RN, El Haibi CP, Jaafar RF, Noureddin BN. Intravitreal bevacizumab vs verteporfin photodynamic therapy for neovascular age-related macular degeneration. *Arch Ophthalmol.* 2007;125:1357–1361.
13. Gelisken F, Lafaut BA, Inhoffen W, Voelker M, Grisanti S, Bartz-Schmidt KU. Clinicopathological findings of choroidal neovascularization following verteporfin photodynamic therapy. *Br J Ophthalmol.* 2004;88:207–211.
14. Schmidt-Erfurth U, Laqua H, Schlotzer-Schrehard U, Viestenz A, Naumann GOH. Histopathological changes following photodynamic therapy in human eyes. *Arch Ophthalmol.* 2002;120:835–844.
15. Moan J, Berg K. The photodegradation of porphyrins in cells can be used to estimate the lifetime of singlet oxygen. *Photochem Photobiol.* 1991;53:549–553.
16. Lange N, Ballini J-P, Wagnieres G, van den Bergh H. A new drug-screening procedure for photosensitizing agents used in photodynamic therapy for CNV. *Invest Ophthalmol Vis Sci.* 2001;42:38–46.
17. Tran TC, Sneed B, Haider J, et al. Automated, quantitative screening assay for antiangiogenic compounds using transgenic zebrafish. *Cancer Res.* 2007;67:11386–11392.
18. Jones PA, King AV. High throughput screening (HTS) for phototoxicity hazard using the in vitro 3T3 neutral red uptake assay. *Toxicol In Vitro.* 2003;17:703–708.
19. Dixit M, West M, Earl L, Lovell W. An in vitro cell culture method for screening of photoirritation using 3T3 neutral red uptake assay. *Toxicol In Vitro.* 1993;8:759–761.
20. Nathalie D, Yannick G, Caroline B, et al. Assessment of the phototoxic hazard of some essential oils using modified 3T3 neutral red uptake assay. *Toxicol In Vitro.* 2006;20:480–489.
21. Sullivan JM. Low-cost monochromatic microsecond flash microbeam apparatus for single-cell photolysis of rhodopsin or other photolabile pigments. *Rev Sci Inst.* 1998;69:527–539.
22. Zorov DB, Filburn CR, Klotz L-O, Zweier JL, Sollott SJ. Reactive oxygen (ROS)-induced ROS release: a new phenomenon accompanying induction of the mitochondrial permeability transition in cardiac myocytes. *J Exp Med.* 2000;192:1001–1014.
23. Detty MR, Prasad PN, Donnelly DJ, Ohulchanskyy T, Gibson SL, Hill R. Synthesis, properties, and photodynamic properties in vitro of heavy-chalcogen analogues of tetramethylrosamine: *Bioorg Med Chem.* 2004;12:2537–2544.
24. Oseroff AR, Ara G, Wadwa KS, Dahl T. Selective photochemotherapy with cationic photosensitizers, In: Kessel D, ed. *Photodynamic Therapy of Neoplastic Disease.* Vol I. Boca Raton, FL: CRC Press; 1990:296–297.
25. Stillman BW, Gluzman Y. Replication and supercoiling of Simian Virus 40 DNA in cell extracts from human cells. *Mol Cell Biol.* 1985;5:2051–2060.
26. Sullivan JM, Satchwell MF. Development of stable cell lines expressing high levels of point mutants of human opsin for biochemical and biophysical studies. *Methods Enzymol.* 2000;315:30–58.
27. Rumyantsev SL, Shur MS, Bilenko Y, Kosterin PV, Salzberg BM. Low frequency noise and long-term stability of noncoherent light sources. *J Appl Opt.* 2004;96:966–969.

28. Soukas NS, Ximenez-Fyvie LA, Hamblin MR, Socransky SS, Hasan T. Targeted antimicrobial photochemotherapy. *Antimicrob Agents Chemother.* 1998;42:2595–2601.
29. Moor ACE. Signaling pathways in cell death and survival after photodynamic therapy. *J Photochem Photobiol B Biol.* 2000;57:1–13.
30. Walter-Yohrling J, Morgenbesser S, Rouleau C, et al. Murine endothelial cell lines as models of tumor endothelial cells. *Clin Canc Res.* 2004;10:2179–2189.
31. Renno RZ, Terada Y, Haddadin MJ, Michaud NA, Gragoudas ES, Miller JW. Selective photodynamic therapy by targeted verteporfin delivery to experimental choroidal neovascularization mediated by a homing peptide to vascular endothelial growth factor receptor-2. *Arch Ophthalmol.* 2004;122:1002–1011.
32. Friedlander M, Theesfeld CL, Sugita M, et al. Involvement of integrins $\alpha_v\beta_3$ and $\alpha_v\beta_5$ in ocular neovascular diseases. *Proc Natl Acad Sci USA.* 1996;93:9764–9769.
33. Mainster M. Wavelength selection in macular photocoagulation, tissue optics, thermal effects, and laser systems. *Ophthalmology.* 1986;93:952–958.
34. Stolz RA, Glazer-Hockstein C, Tolentino MJ, Maguire AM. Transmission of retinal laser wavelengths through blood. *Retina.* 2005; 25:498–502.
35. Allison RR, Mota HC, Bagnato VS, Sibata CH. Bio-nanotechnology and photodynamic therapy: state of the art review. *Photodiagnosis Photodyn Ther.* 2008;5:19–38.
36. Rolling F, Nong Z, Collen D. Adeno-associated virus-mediated gene transfer into rat carotid arteries. *Gene Therapy.* 1997;4:757–761.
37. Nicklin SA, Buening H, Dishart KL, de Alwis M, Girod A, et al. Efficient and selective AAV2-mediated gene transfer directed to human vascular endothelial cells. *Mol Therapy.* 2001;4:174–181.
38. Suh W, Han S-O, Ya L, Kim SW. An angiogenic, endothelial-cell-targeted polymeric gene carrier. *Mol Ther.* 2002;6:664–672.
39. Zhu C, Zhang Y, Pardridge WM. Widespread expression of an exogenous gene in the eye after intravenous administration. *Invest Ophthalmol Vis Sci.* 2002;43:3075–3080.
40. Ideta R, Yanagi Y, Tamaki Y, Tasaka F, Harada A, Kataoka K. Effective accumulation of polyion complex micelle to experimental choroidal neovascularization in rats. *FEBS Lett.* 2004;537:21–25.
41. Ogawara K-I, Rots MG, Kok RJ, et al. A novel strategy to modify adenovirus tropism and enhance transgene delivery to activated vascular endothelial cells in vitro and in vivo. *Hum Gene Ther.* 2004;15:433–443.
42. White SJ, Nicklin SA, Buning H, et al. Targeted gene delivery to vascular tissue in vivo by tropism-modified adeno-associated virus vectors. *Circulation.* 2004;109:513–519.
43. Treynor TP, Vizcarra CL, Nedelcu D, Mayo SL. Computationally designed libraries of fluorescent proteins evaluated by preservation and diversity of function. *Proc Natl Acad Sci USA.* 2007;104:48–53.